



## Article

# Facile Preparation of Pd/UiO-66-v for the Conversion of Furfuryl Alcohol to Tetrahydrofurfuryl Alcohol under Mild Conditions in Water

Yanliang Yang <sup>1,\*</sup> , Dongsheng Deng <sup>1</sup>, Dong Sui <sup>1</sup>, Yanfu Xie <sup>2</sup>, Dongmi Li <sup>1</sup> and Ying Duan <sup>2,\*</sup>

<sup>1</sup> Henan Key Laboratory of Function-Oriented Porous Material, College of Chemistry and Chemical Engineering, Luoyang Normal University, Luoyang 471934, China; dengdongsheng168@sina.com (D.D.); suidonghy@mail.nankai.edu.cn (D.S.); lidongmi223@126.com (D.L.)

<sup>2</sup> College of Food and Drug, Luoyang Normal University, Luoyang 471934, China; xieyanfu1234@163.com

\* Correspondence: yangyli@mail.ustc.edu.cn (Y.Y.); duanying@mail.ustc.edu.cn (Y.D.); Tel.: +86-379-6861-8320 (Y.Y.); +86-379-6861-8516 (Y.D.)

Received: 12 November 2019; Accepted: 26 November 2019; Published: 28 November 2019



**Abstract:** The hydrogenation of furan ring in the biomass-derived furans is of great importance for the conversion of biomass to valuable chemicals. Fabrication of high activity and selectivity catalyst for this hydrogenation under mild conditions was one of the focuses of this research. In this manuscript, UiO-66-v, in which vinyl bonded to the benzene ring, was first prepared. Then, the uniformly distributed vinyl was used as the reductant for the preparation of Pd/UiO-66-v. The catalyst was characterized by X-ray diffraction, thermogravimetric, N<sub>2</sub> physical adsorption/desorption, X-ray photoelectron spectroscopy, scanning electron microscope, transmission electron microscopy, energy dispersive spectrometer elemental mappings, and inductively coupled plasma atomic emission spectroscopy to find the Pd/UiO-66-v had a narrow palladium nanoparticles size of 3–5 nm and maintained the structure and thermal stability of UiO-66-v. The Pd/UiO-66-v was used for the hydrogenation of furfuryl alcohol to tetrahydrofurfuryl alcohol in water. 99% conversion of furfuryl alcohol was obtained with 90% selectivity to tetrahydrofurfuryl alcohol after reacted at 0.5 MPa H<sub>2</sub>, 303 K for 12 h. The Pd/UiO-66-v was proved to be effective for the hydrogenation of furan ring in furans and could be used for at least five times.

**Keywords:** furfuryl alcohol; hydrogenation; tetrahydrofurfuryl alcohol; Pd/UiO-66-v; water solvent

## 1. Introduction

Furfural, a renewable compound from dehydration of pentoses, is produced in millions of tons scale in industry every year. Furfural was called gold from garbage, as most of the raw material for the production of furfural was agricultural waste such as corncobs, cotton hulls, sugar cane bagasse, and more [1]. The conversion of furfural to valuable chemicals was attracting more attention as the consuming in fossil resources [2–7]. The main products from furfural were cyclopentanone [8–12], furfuryl alcohol (FA) [13–16], tetrahydrofurfuryl alcohol (THFA) [17–30], 1,2-pentanediol [31–35], furan [36,37], and methyl furan [38]. The THFA was a typical product from furfural through the hydrogenation of C=C and C=O in furfural. The THFA is a transparent low toxic liquid of high boiling point and is miscible with water. The THFA could be a good candidate for green solvent due to the high chemical and thermal stability as well as biologic degradability. The THFA is also an intermediate for high value-added compounds such as pyridine [39], dihydropyran [40], and tetrahydrofuran [41]. Additionally, it was reported that 1,5-pentanediol, a promising monomer for the plastics industry, could be obtained from the hydrogenolysis of THFA [42–46].

There was plenty of literature dealing with the conversion of furfural to THFA directly or via FA as an intermedia in two steps. Tomishige et al. gave a report on the direct conversion of furfural to THFA on Ni/SiO<sub>2</sub> with Ni particle size <4 nm. The yield of THFA could reach 94% [19]. They also found that the reaction could be conducted in the aqueous phase catalyzed by Pd-Ir/SiO<sub>2</sub> [18]. Guan et al. achieved the total hydrogenation of furfural to THFA by the physical mix of Pd/Al<sub>2</sub>O<sub>3</sub> and Ru/ZrO<sub>2</sub> [20]. The reaction could be conducted under mild conditions and was believed to proceed with tetrahydrofurfural as intermediate. FA was the main product from the selective hydrogenation of furfural with mature technology in industrial. The conversion of FA to THFA suffered the scientific problem of the hydrogenation of the furan ring, while both the aldehyde and furan ring should be hydrogenated in the process for the conversion of furfural to THFA directly. As a result, the conversion of FA to THFA was of great importance both in industrial and theoretical. More moderate conditions may be needed in the conversion of FA to THFA. Wang et al. performed this conversion using NiCo bimetallic alloy as catalysts. The synergistic effect in the CoNi alloy was responded for the high performance, and 99% yield of THFA was obtained at 353 K, 3 MPa H<sub>2</sub> in ethanol [25]. Guan et al. got 98% conversion of FA and 98% selectivity to tetrahydrofurfuryl alcohol under mild condition in ethanol [47]. In a survey of literature, the yield of THFA could reach a high value in both the direct hydrogenation of furfural procedure and the two steps procedure via FA as an intermedia [17–30]. The weakening of the dependence on harsh reaction conditions (high temperature and pressure, organic solvent) was one of the interest points for the production of THFA.

Due to the high specific surface area, three-dimensional uniform pore structure and easy to be functionalized, the metal organic frameworks (MOFs) had emerged as an excellent candidate for catalyst or support [48–53]. The combination of metal nanoparticles and MOFs often gave the production of high-performance catalysts. Liang et al. prepared Pd@MIL-101(Cr)-NH<sub>2</sub> for the hydrogenation of furfural in water [21]. Near 100% yield of THFA was obtained at 313 K, 2 MPa H<sub>2</sub>. Hensen et al. obtained Ru/UiO-66 through the reduction of RuCl<sub>3</sub> by N<sub>2</sub>H<sub>4</sub>·H<sub>2</sub>O [14]. The Ru/UiO-66 showed high activity in the hydrogenation of furfural to FA. During the preparation of MOFs supported metal nanoparticles, the mild conditions, low temperature, and near-neutral pH for the reduction of metal precursors was a favor to avoid the potential damage and impact on structures of MOFs. In our previous work, the alkenyl was proven to be an ideal reductant for PdCl<sub>2</sub> [54–57]. The reduction reaction could conduct at room temperature in neutral water. Herein, we gave a report on the preparation of Zr-MOF with UiO-66 topology by the condensation of 2-vinylterephthalic acid and zirconium tetrachloride. As the uniform distribution of vinyl in the synthesized UiO-66-v, uniform dispersion of Pd nanoparticles were acquired by just stirring the mixture of PdCl<sub>2</sub> solution and as-synthesized UiO-66-v for 12 h. The prepared Pd/UiO-66-v exhibited high activity for the conversion of FA to THFA at 303 K, 0.5 MPa H<sub>2</sub> in water.

## 2. Materials and Methods

### 2.1. Materials

FA was obtained from Sinopharm Chemical Reagent Co., Ltd., Shanghai, China. Before being used, the FA was purified by vacuum distillation. PdCl<sub>2</sub>, ZrCl<sub>4</sub>, 2-methylfuran and 2,5-dimethylfuran was bought from J&K Chemical Ltd. Beijing, China, 2-vinylterephthalic acid was obtained from Zhengzhou alpha Chemical Co., Ltd. Zhengzhou, China, N, N-Dimethylformamide (DMF), ethanol, NaBH<sub>4</sub>, 5-methyl furfural, and 5-hydroxymethylfurfural was purchased from Aladdin Chemistry Co. Ltd. Shanghai, China. The 5-methylfuran-2-methanol and 2,5-di(hydroxymethyl)furan were prepared by the reduction of 5-methyl furfural and 5-hydroxymethylfurfural by NaBH<sub>4</sub>. Unless otherwise specified, the reagent was used as received.

## 2.2. Preparation of Catalysts

UiO-66-v was prepared according to the previous report [58]. Typically,  $\text{ZrCl}_4$  was first dissolved in a mixture solvent of DMF and HCl ( $V_{\text{DMF}}:V_{\text{HCl}} = 5:1$ , 15 mL) and then 2-vinylterephthalic acid (2.0 mmol) dissolved in DMF (25 mL) was added into the mixture and sonicated for 20 min. After that, the mixture was transferred into a 50 mL Teflon-lined steel autoclave. The autoclave was heated to 353 K and kept at 353 K for 12 h and then cooled to room temperature naturally. The white mixture was washed first by DMF (50 mL  $\times$  2) and then ethanol (50 mL  $\times$  3). The UiO-66 was obtained as a white powder after the precipitate was dried under a vacuum for 12 h at 363 K.

Pd/UiO-66-v was prepared through the reduction of  $\text{PdCl}_2$  by vinyl at mild conditions. Typically, UiO-66-v (0.20 g) was added to water (50 mL) and stirred for 30 min at 353 K. Then, dilute hydrochloric acid aqueous solution of  $\text{PdCl}_2$  (Pd: 0.5 wt.%, 1.00 g) was added to the mixture and stirred for another 12 h at 353 K to afford black precipitate. The precipitate was first washed with water (50 mL  $\times$  3) and then ethanol (50 mL  $\times$  3). Finally, it was dried under a vacuum for 12 h at 363 K.

## 2.3. Characterization of Catalysts

The powder X-ray diffraction (XRD) patterns were obtained on a Rigaku D/Max 2500/PC powder diffractometer (Tokyo, Japan) at a scanning rate of  $5^\circ \cdot \text{min}^{-1}$  using Cu  $K\alpha$  radiation ( $\lambda = 0.15418$  nm) at 40 kV and 40 mA. The thermogravimetric (TG) analysis was conducted on PerkinElmer Diamond TG/DTA6300 (Waltham, MA, USA). The temperature range was 323 K to 1073 K with the heating rate was  $5 \text{ K} \cdot \text{min}^{-1}$ . The  $\text{N}_2$  physical adsorption/desorption curves were collected on a Micromeritics ASAP 2040 apparatus (Narcross, GA, USA). Before measurement, the samples (50.0 mg) were pretreated at 423 K. The X-ray photoelectron spectroscopy (XPS) spectra were collected on a Thermo Fisher K-alpha (Waltham, MA, USA) with an Al  $K\alpha$  (1486.6 eV) radiation source. The pass energy was 200.0 eV for survey scan while 50 eV for high-resolution spectrum. The peak areas were constraint as  $3d_{5/2}:3d_{3/2} = 3:2$  and  $2p_{3/2}:2p_{1/2} = 2:1$ . The 80% Lorentzian-Gaussian was selected as the shape line. The scanning electron microscope (SEM) images were taken on FEI Nova Nano-SEM (Hillsboro, OR, USA) with 20 kV HD. Transmission electron microscopy (TEM) images were taken by FEI Tecnai G2 F20 microscope (Hillsboro, OR, USA) with 200 kV accelerating voltage. The high-resolution transmission electron microscope (HRTEM) and energy dispersive spectrometer (EDS) elemental mappings were taken by JEM-2100F (Tokyo, Japan) equipped with an Oxford x-met8000 detector. Before test, the sample was ultrasonic in ethanol. The content of Pd was determined by inductively coupled plasma atomic emission spectroscopy (ICP-AES) by Agilent 7700 (Santa Clara, CA, USA).

## 2.4. Catalytic Reactions

The catalytic reaction was taken in a 20 mL stainless-steel autoclave with a glass lining. In a typical procedure, FA aqueous solution (1 mmol, 2 mL), Pd/UiO-66-v (10.0 mg) and magneton was added into the autoclave. After sealed and purged with  $\text{H}_2$  for four times to exclude the air, the autoclave was inflated with  $\text{H}_2$  to the desired pressure. The autoclave was then put in a magnetic stirring oil bath at 303 K for a certain time. After the reaction, internal standard (decane) was added into the mixture and then the mixture was diluted by ethanol. The liquid phase was collected for analysis after centrifugation. The turnover frequency (TOF) was calculated based on all the Pd atoms in the catalysts and the whole reaction time.

## 2.5. Product Analysis

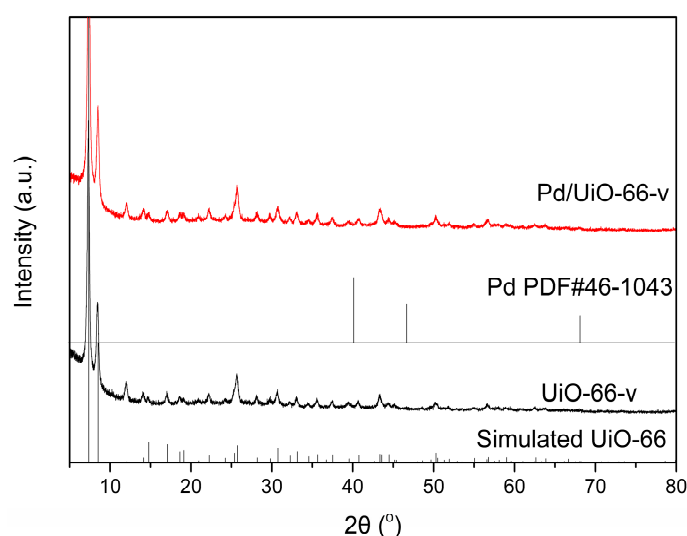
The qualitative analysis was conducted by GC on a Shimadzu GC-2014 (Tokyo, Japan) equipped with a SH-Rtx-5 column (30 m  $\times$  0.32 mm  $\times$  0.25  $\mu\text{m}$ ). The column oven was first kept at 333 K for 4 min and then increased to 523 K at a rate of  $20 \text{ K} \cdot \text{min}^{-1}$  and kept at 523 K for 1.5 min. Decane was used as the internal standard. The qualitative analysis was performed on Shimadzu GC/MS-TQ8040 (Tokyo, Japan) equipped with an InerCap 17MS column (30 m  $\times$  0.25 mm  $\times$  0.25  $\mu\text{m}$ ). The column oven

was first kept at 323 K for 1 min, and then increased to 473 K at a rate of  $40\text{ K}\cdot\text{min}^{-1}$  and increased to 553 K at a rate of  $15\text{ K}\cdot\text{min}^{-1}$  and kept at 553 K for five min. The obtained mass spectrum was shown in Supplementary Materials (Figures S1–S7).

### 3. Results and Discussion

#### 3.1. Catalyst Characterization

The Zr-MOF was prepared according to the previous reported procedure with modification that the 2-vinylterephthalic acid was used instead of terephthalic acid for the preparation of UiO-66-v. The XRD pattern of UiO-66-v showed that the as-synthesized Zr-MOF have the topology of UiO-66 comparing to the XRD pattern of simulated UiO-66 (Figure 1). The Pd was introduced to the UiO-66-v by the reaction of  $\text{PdCl}_2$  and vinyl in the UiO-66-v in water. The reduction procedure could be conducted just by stirring the UiO-66-v in the aqueous solution of  $\text{PdCl}_2$ . As no harsh conditions such as high temperature or base was needed, the resulted Pd/UiO-66-v maintained the frame structure of UiO-66-v. No difference could be observed between the XRD patterns of UiO-66-v and Pd/UiO-66-v (Figure 1). Additionally, no crystal plane diffraction peak corresponding to metallic Pd was founded in the XRD pattern of Pd/UiO-66-v. To find out why there was no signal for Pd in the XRD pattern, the HRTEM picture of Pd/UiO-66-v was taken (Figure S8). It was found that not all the Pd nanoparticles had good crystallinity. Part of the Pd nanoparticles had amorphous state. On the other hand, the ICP-AES showed the Pd content was 2.42 wt.% (Table 1, Entry 2). Based on these, the absence of Pd signal in the XRD pattern should be caused by the low content of Pd, the amorphous state for part of the Pd nanoparticles and the small particle size of Pd. The thermal stability of UiO-66-v and Pd/UiO-66-v was studied by the thermogravimetric analysis, and the results were shown in Figure S9. There had a little weight loss at 373 K in both samples, which should be caused by the residual solvent in the samples during the preparation process. Then, the two samples had sharp weight loss when the temperature was close to 773 K. This was caused by the decomposition of UiO-66-v at this temperature. The results showed the high thermal stability for the framework of UiO-66-v and the introduction of Pd did not affect the stability of UiO-66-v.



**Figure 1.** The XRD patterns of UiO-66-v, Pd/UiO-66-v, simulated UiO-66, and Pd PDF#46-1043.

The BET surface area and pore structure of as-synthesized UiO-66-v and Pd/UiO-66-v were characterized by  $\text{N}_2$  adsorption/desorption isotherms as shown in Figure 2. The BET surface was  $862\text{ m}^2\cdot\text{g}^{-1}$  for UiO-66-v, which was closed to that for the UiO-66 modified with a single group ( $-\text{NH}_2$ ,  $-\text{NO}_2$  and  $-\text{OH}$ ) reported in the literature (Table 1, Entry 1) [58–60]. The micropore area was calculated by the t-plot method and the area was  $726\text{ m}^2\cdot\text{g}^{-1}$ , indicating the surface area was most contributed

by the micropore area. After the introduction of Pd, both the BET surface area and the micropore area calculated by the t-plot method decreased slightly and was accompanied by the decrease in pore volume. The reason should be the in presence of partly Pd in the pore of UiO-66. The practice Pd content was determined by ICP-AES, and the value (2.42 wt.%) was very close to the theoretical value (Table 1, Entry 2). After reaction, the Pd content was maintained showed the catalyst was stable under the mild reaction conditions (2.35 wt.%).

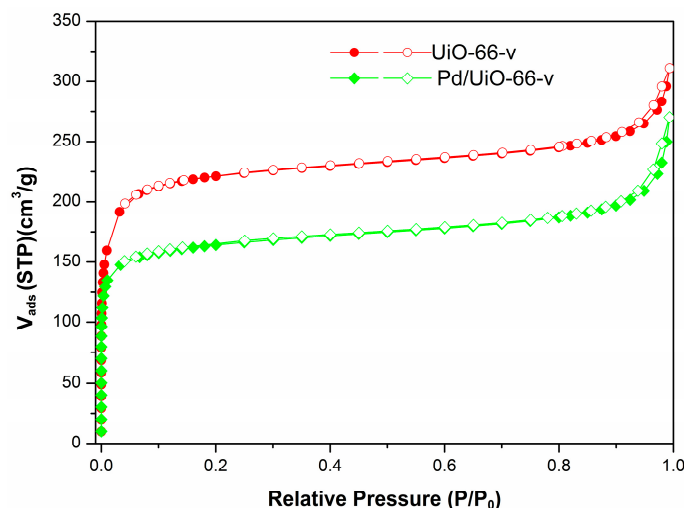


Figure 2.  $N_2$  adsorption/desorption isotherms of the UiO-66-v and Pd/UiO-66-v.

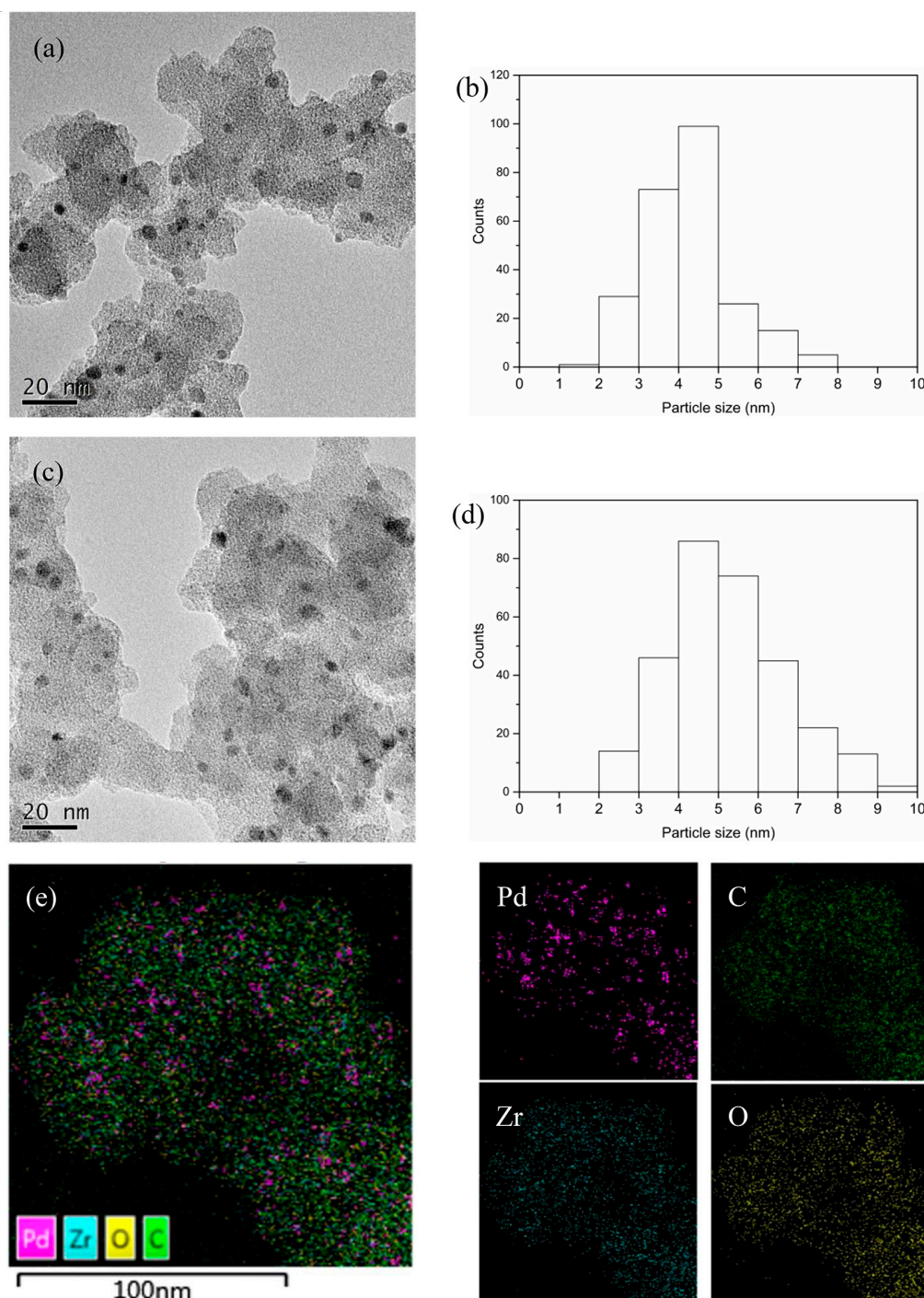
Table 1. The structural properties of as-synthesized samples.

Entry	Sample	$S_{BET}$ ( $m^2 \cdot g^{-1}$ )	$S_{t-plot}$ ( $m^2 \cdot g^{-1}$ )	PV <sup>1</sup> ( $cm^3 \cdot g^{-1}$ )	PV <sup>2</sup> ( $cm^3 \cdot g^{-1}$ )	Pd Content <sup>3</sup> (wt.%)
1	UiO-66-v	862	726	0.42	0.28	-
2	Pd/UiO-66-v	630	514	0.41	0.20	2.42 (2.35) <sup>4</sup>

<sup>1</sup> Total pore volume, <sup>2</sup> t-Plot micropore volume, <sup>3</sup> determined by the ICP-AES characterization, <sup>4</sup> Numbers in brackets referred to the Pd content for used catalyst.

The morphology of samples was characterized by the electron microscope. The UiO-66-v and Pd/UiO-66-v both crystallized nanocrystals with a size distribution of around 80 nm revealed by the scanning electron microscope (SEM) image (Figures S10 and S11). The introduction of Pd had no influence on the morphology of UiO-66-v based on the SEM results. The Pd nanoparticles had a narrow size distribution between 3–5 nm by counting the diameters of about 250 Pd nanoparticles in several transmission electron microscope (TEM) images (Figure 3, Figure S12, and Figure S13). The narrow size distribution of Pd should be caused by the uniform distribution of the reductant. The EDS elemental mappings for Pd/UiO-66-v also showed that the Pd homogenously distributed in the sample (Figure 3e, Figure S14, and Figure S15). The vinyl, used as the reductant, was linked by the carbon-carbon bond to the benzene ring in the structure of UiO-66-v. The number of metallic Pd atoms is limited in a given region caused by the limited number of vinyl for the reduction reaction of  $PdCl_2$ . The used catalyst was characterized by the TEM. The Pd nanoparticles maintained the narrow size distribution, but enlarged slightly after the reaction (Figure 3c,d).

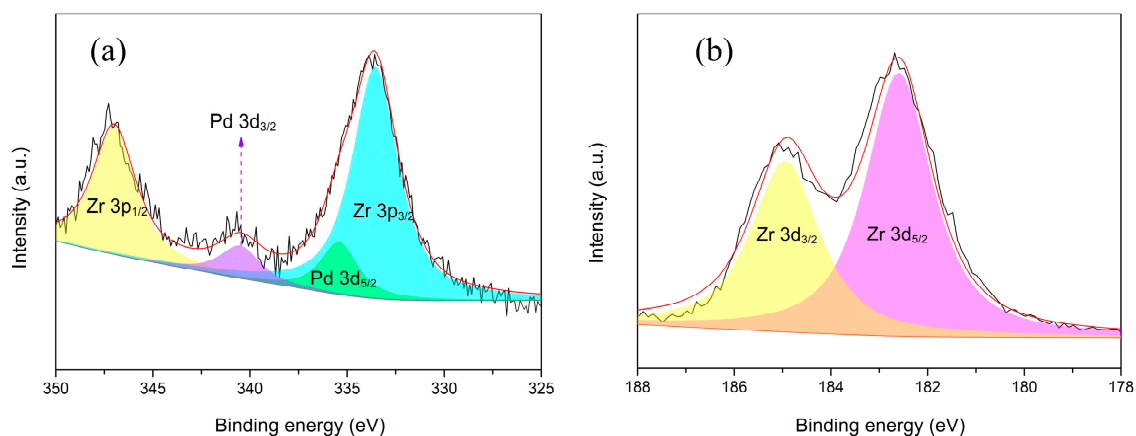




**Figure 3.** The TEM images and the corresponding particle size distribution of Pd/UiO-66-v (a,b) and the used catalyst (c,d) and the EDS mappings for Pd/UiO-66-v (e).

The surface chemical composition of Pd/UiO-66-v was characterized by X-ray photoelectron spectroscopy (XPS). The survey scan showed the surface was composed of Pd, Zr, C, and O (Figure S16). There was partial overlap in the high-resolution spectrum of Pd 3d and Zr 3p (Figure 4a, Table 2). After the curve fitting process, two binding energy peaks centered at 335.4 eV and 340.6 eV were observed corresponding to the 3d<sub>5/2</sub> and 3d<sub>3/2</sub> of Pd(0), respectively [59–61]. The low doublet separation for Pd (5.2 eV) should be caused by the interaction between Pd and Zr. Obviously, the PdCl<sub>2</sub> was reduced to Pd(0) successfully by the vinyl. The additional two peaks at 333.5 eV and 347.0 eV could be assigned to the Zr 3p<sub>3/2</sub> and 3p<sub>1/2</sub>, respectively [59,60]. The presence of Zr was also proved by

the binding energy peaks at 182.6 eV and 185.0 eV in the high-resolution spectrum of Zr (Figure 4b, Table 2). The two peaks corresponding to the 3d<sub>5/2</sub> and 3d<sub>3/2</sub> of Zr [59,60].



**Figure 4.** XPS spectra of Pd/UiO-66-v: high-resolution spectrum of Pd 3d (a) and Zr 3d (b).

**Table 2.** The binding energy for Pd and Zr in Pd/UiO-66-v.

Element	Pd 3d <sub>5/2</sub>	Pd 3d <sub>3/2</sub>	Zr 3p <sub>3/2</sub>	Zr 3p <sub>1/2</sub>	Zr 3d <sub>5/2</sub>	Zr 3d <sub>3/2</sub>
B.E. (eV)	335.4	340.6	333.5	347.0	182.6	185.0

### 3.2. Hydrogenation of Furfuryl Alcohol

The Pd/UiO-66-v showed high activity in the hydrogenation of FA to THFA. The conversion was very low (<1%) when the reaction was conducted without any catalysts (Table 3, Entry 1). When the UiO-66-v without the introduction of Pd was used as catalysts, the conversion was also very low (2%) (Table 3, Entry 2). This showed that the Pd was responded for the conversion of FA. The hydrogenation reaction was then performed in 0.5 MPa H<sub>2</sub> at 303 K in water in the presence of Pd/UiO-66-v. After reacted for 2 h, 28% of FA was converted with 92% selectivity to THFA (Table 3, Entry 3). As the H<sub>2</sub> pressure increased from 0.5 MPa to 4 MPa, the conversion of FA increased from 28% to 92% while the selectivity to THFA kept around 90% (Table 3, Entries 3–7). On the other hand, when the reaction time was prolonged to 12 h at 0.5 MPa H<sub>2</sub>, the FA was converted almost completely with 90% selectivity to THFA (Table 3, Entry 8). The results showed the Pd/UiO-66-v was very effective for the hydrogenation of FA to THFA, even at mild conditions in water. The selectivity kept stand as the reaction time prolonged was also proved by the reaction progress profiles reacted at 4 MPa H<sub>2</sub> (Figure S17). As the reaction time increased from 0.5 h to 2.5 h, the conversion of FA increased from 27% to 99%. The selectivity to THFA kept around 90% as the increasing reaction time. The effect of the solvent on the hydrogenation of FA was studied. When alcohols were used as the solvent, the selectivity to THFA maintained while the conversion decreased a lot. This decrease in activity should be interpreted from the perspective of the interaction between solvent and FA based on our recent work [57]. The FA had stronger interaction with alcohols than with water. When the alcohols were used as solvents, more energy was needed for the FA to get off the solvent to the surface of catalyst than in water solvent. This difference in energy demands should be responding for the different activity in alcohols or water, especially at a lower temperature. The water was the most suitable solvent for the hydrogenation of FA on Pd/UiO-66-v.

**Table 3.** Hydrogenation of FA under different solvent, pressure, and reaction time <sup>1</sup>.

Entry	Catalysts	Solvent	P (MPa)	Time (h)	Conversion (%)	Selectivity (%)	Carbon Balance
1	None	H <sub>2</sub> O	4	2	<1	n.d.	>99
2	UiO-66-v	H <sub>2</sub> O	4	2	2	n.d.	98
3	Pd/UiO-66-v	H <sub>2</sub> O	0.5	2	28	92	98
4	Pd/UiO-66-v	H <sub>2</sub> O	1	2	52	91	95
5	Pd/UiO-66-v	H <sub>2</sub> O	2	2	79	90	92
6	Pd/UiO-66-v	H <sub>2</sub> O	3	2	88	90	91
7	Pd/UiO-66-v	H <sub>2</sub> O	4	2	92	91	92
8	Pd/UiO-66-v	H <sub>2</sub> O	0.5	12	99	90	90
9	Pd/UiO-66-v	methanol	4	2	14	94	99
10	Pd/UiO-66-v	ethanol	4	2	38	93	97
11	Pd/UiO-66-v	isopropanol	4	2	2	96	>99

<sup>1</sup> Reaction conditions: FA solution (1 mmol, 2 mL), 303 K, Pd/UiO-66-v (0.228 mol%, 10.0 mg) or UiO-66-v (10.0 mg), methyltetrahydrofuran and dimer (2,2'-(oxybis(methylene))difuran) were detected as by products, n.d. (not detected).

The effect of substrate concentration on the hydrogenation of FA was investigated by changing the concentration of FA with the same catalyst loading. When the reaction time was restricted at 2 h, the TOF for the hydrogenation of FA first increased from 202 h<sup>-1</sup> to 286 h<sup>-1</sup> when the concentration increased from 0.5 mol L<sup>-1</sup> to 1.0 mol L<sup>-1</sup> (Table 4, Entries 1,2). Then, the TOF decreased as the concentration continued to rise (Table 4). So, the concentration of 1.0 mol·L<sup>-1</sup> should be the suitable concentration for this reaction when using Pd/UiO-66-v as the catalyst in water. However, a TOF as high as 187 h<sup>-1</sup> was obtained at a concentration of 2.5 mol L<sup>-1</sup>. This showed that the catalyst could work at a higher concentration of FA. To test whether a higher conversion could be obtained at a high concentration of FA, the reaction time was prolonged for a different concentration of FA. 96% conversion of FA with 86% selectivity to THFA was acquired after 4 h when the concentration of FA was 1.0 mol·L<sup>-1</sup> (Table 4, Entry 3). The TOF was 211 h<sup>-1</sup> which was lower than only reacted for 2 h. A similar decrease in TOF was also observed at higher concentration of FA. 88%, 73%, and 58% conversion of FA were respectively obtained when the concentration of FA increased from 1.5 mol·L<sup>-1</sup> to 2.5 mol·L<sup>-1</sup> (Table 4, Entries 5, 7, and 9). The TOF was 193 h<sup>-1</sup>, 161 h<sup>-1</sup>, and 128 h<sup>-1</sup>, respectively, which was lower than the value obtained at 2 h. The TOF should relate to the concentration of FA. As the time prolonged, the concentration of FA decreased, which led to the decrease in TOF. The selectivity to THFA was between 83% and 91%, showing the high selectivity to the hydrogenation furan rings.

**Table 4.** Effect of concentration on the hydrogenation of FA to THFA <sup>1</sup>.

Entry	C (mol·L <sup>-1</sup> )	Time (h)	TOF (h <sup>-1</sup> )	Conversion (%)	Selectivity (%)	Carbon Balance
1	0.5	2	202	92	91	92
2	1.0	2	286	65	90	94
3	1.0	4	211	96	86	87
4	1.5	2	257	39	88	95
5	1.5	6	193	88	85	87
6	2.0	2	255	29	89	97
7	2.0	8	161	73	83	88
8	2.5	2	187	17	91	98
9	2.5	10	128	58	83	90

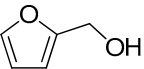
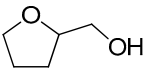
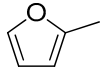
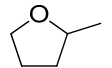
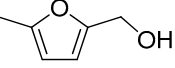
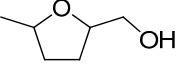
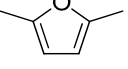
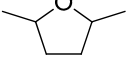

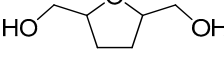
<sup>1</sup> Reaction conditions: FA aqueous solution (2 mL), 4 MPa H<sub>2</sub>, 303 K, Pd/UiO-66-v (0.228 mol%, 10.0 mg), methyltetrahydrofuran and dimer (2,2'-(oxybis(methylene))difuran) were detected as by products. TOF: moles of FA converted/ (time × moles of Pd).

The Pd/UiO-66-v was used to hydrogenate different furan compounds to investigate the ability for hydrogenation of furan ring. As the 2-methylfuran, 2,5-dimethylfuran, and 5-methylfuran-2-methanol were insoluble in water, the hydrogenation reaction was conducted in ethanol. The conversion of 2-methylfuran was 99% after 2.5 h, even in ethanol. The selectivity



to 2-methyltetrahydrofuran was 90% (Table 5, Entry 2). When 5-methylfuran-2-methanol, 2,5-dimethylfuran, and 2,5-di(hydroxymethyl)furan were used as the substrate, the compounds could not be transformed completely in 2.5 h (Table 5, Entries 3–5). The main product was the compounds of hydrogenation of the furan ring. To get high conversion of 5-methylfuran-2-methanol, 2,5-dimethylfuran, and 2,5-di(hydroxymethyl)furan, the reaction time was prolonged to 24 h. The conversion for the three furan derivatives was over 95% with the main product of the hydrogenation of furan ring (Table 5, Entries 3–5). Those results showed the Pd/UiO-66-v possessed high activity and selectivity for the hydrogenation of the furan ring.

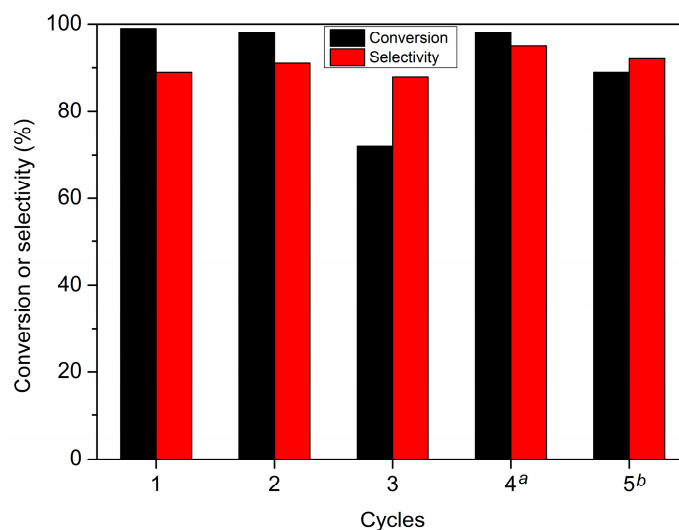
**Table 5.** Hydrogenation of furan derivatives on Pd/UiO-66-v <sup>1</sup>.

Entry	Substrate	Solvent	Conversion (%) <sup>2</sup>	Selectivity (%) <sup>2</sup>	Carbon Balance
1		H <sub>2</sub> O	99	 89	89
2		ethanol	99	 90	90
3		ethanol	44 (97)	 93 (91)	97 (91)
4		ethanol	11 (98)	 90 (90)	99 (90)
5		H <sub>2</sub> O	18 (99)	 95 (92)	99 (92)

<sup>1</sup> Reaction conditions: furan derivatives solution (2 mL), Pd/UiO-66-v (0.228 mol%, 10.0 mg), 303 K, 2 MPa H<sub>2</sub>, 2.5 h.

<sup>2</sup> Numbers in brackets referred to the reaction time of 24 h.

The reuse performance of Pd/UiO-66-v was investigated by catalyst recycling experiments (Figure 5). The catalyst was recovered and washed by ethanol and water after the reaction and used for the next cycle. The selectivity to THFA kept around 90% in all the cycles, however, the conversion decreased to 72% in the third use. This decrease should be mainly ascribed to the loss of catalyst in the recovery process. We increased the reaction time to 3.5 h in the next cycle and the conversion increased to 98%, with 95% selectivity to THFA. The conversion was 89% with 92% selectivity to THFA in the fifth cycle after 4 h.



**Figure 5.** Cycle experiments for the hydrogenation of FA in water. <sup>a</sup> reaction time was 3.5 h. <sup>b</sup> reaction time was 4 h.

#### 4. Conclusions

In conclusion, UiO-66-v with vinyl in the benzene ring was successfully synthesized. The uniformly distributed vinyl was an effective reductant for the facile preparation of Pd/UiO-66-v with a narrow size distribution of Pd nanoparticles. The frame structure and high thermal stability was maintained after the introduction of Pd into UiO-66-v. The Pd/UiO-66-v showed high activity and selectivity for the hydrogenation of FA to THFA under mild conditions and could be used for the hydrogenation of furan ring in a series of furan derivatives. The Pd/UiO-66-v could be used for five times with no decrease in selectivity.

**Supplementary Materials:** The following are available online at <http://www.mdpi.com/2079-4991/9/12/1698/s1>, Figures S1–7. Mass spectrum, Figure S8. The HRTEM picture of Pd/UiO-66-v, Figure S9. The TG curves for UiO-66-v and Pd/UiO-66-v, Figure S10. The SEM image for UiO-66-v, Figure S11. The SEM image for Pd/UiO-66-v, Figure S12. The TEM image for Pd/UiO-66-v, Figure S13. The TEM image for used Pd/UiO-66-v, Figure S14. The electron image for Pd/UiO-66-v, Figure S15. The map sum spectrum for Pd/UiO-66-v, Figure S16. The survey XPS spectra of Pd/UiO-66-v, Figure S17. Influence of reaction time on the hydrogenation of furfuryl alcohol.

**Author Contributions:** Conceptualization, Y.Y. and D.D.; methodology Y.Y., D.S. and Y.X., writing—original draft preparation, D.L.; writing—review and editing, Y.Y.; visualization, D.S.; supervision, Y.D.; funding acquisition, Y.Y. and Y.D.

**Funding:** This work was supported by the National Natural Science Foundation of China (21902071 and 21801110) and Science and Technology Research Project of Henan Province (192102210160).

**Conflicts of Interest:** The authors declare no conflict of interest.

#### References

1. Win, D.T. Furfural-gold from garbage. *AU J. Technol.* **2005**, *8*, 185–190.
2. Li, X.; Jia, P.; Wang, T. Furfural: A promising platform compound for sustainable production of C<sub>4</sub> and C<sub>5</sub> chemicals. *ACS Catal.* **2016**, *6*, 7621–7640. [[CrossRef](#)]
3. Lange, J.P.; van der Heide, E.; van Buijtenen, J.; Price, R. Furfural—A promising platform for lignocellulosic biofuels. *ChemSusChem* **2012**, *5*, 150–166. [[CrossRef](#)] [[PubMed](#)]
4. Mariscal, R.; Maireles-Torres, P.; Ojeda, M.; Sádaba, I.; Granados, M.L. Furfural: A renewable and versatile platform molecule for the synthesis of chemicals and fuels. *Energy. Environ. Sci.* **2016**, *9*, 1144–1189. [[CrossRef](#)]
5. Wang, Y.; Zhao, D.; Rodríguez-Padrón, D.; Len, C. Recent advances in catalytic hydrogenation of furfural. *Catalysts* **2019**, *9*, 796. [[CrossRef](#)]
6. Chen, S.; Wojcieszak, R.; Dumeignil, F.; Marceau, E.; Royer, S. How catalysts and experimental conditions determine the selective hydroconversion of furfural and 5-hydroxymethylfurfural. *Chem. Rev.* **2018**, *118*, 11023–11117. [[CrossRef](#)]
7. Gupta, K.; Rai, R.K.; Singh, S.K. Metal catalysts for the efficient transformation of biomass-derived HMF and furfural to value added chemicals. *ChemCatChem* **2018**, *10*, 2326–2349. [[CrossRef](#)]
8. Li, Y.; Guo, X.; Liu, D.; Mu, X.; Chen, X.; Shi, Y. Selective conversion of furfural to cyclopentanone or cyclopentanol using Co-Ni catalyst in water. *Catalysts* **2018**, *8*, 193. [[CrossRef](#)]
9. Zhang, G.-S.; Zhu, M.-M.; Zhang, Q.; Liu, Y.-M.; He, H.-Y.; Cao, Y. Towards quantitative and scalable transformation of furfural to cyclopentanone with supported gold catalysts. *Green Chem.* **2016**, *18*, 2155–2164. [[CrossRef](#)]
10. Yang, Y.; Du, Z.; Huang, Y.; Lu, F.; Wang, F.; Gao, J.; Xu, J. Conversion of furfural into cyclopentanone over Ni-Cu bimetallic catalysts. *Green Chem.* **2013**, *15*, 1932–1940. [[CrossRef](#)]
11. Li, X.-L.; Deng, J.; Shi, J.; Pan, T.; Yu, C.-G.; Xu, H.-J.; Fu, Y. Selective conversion of furfural to cyclopentanone or cyclopentanol using different preparation methods of Cu-Co catalysts. *Green Chem.* **2015**, *17*, 1038–1046. [[CrossRef](#)]
12. Hronec, M.; Fulajtarová, K. Selective transformation of furfural to cyclopentanone. *Catal. Commun.* **2012**, *24*, 100–104. [[CrossRef](#)]

13. Ruan, L.; Zhang, H.; Zhou, M.; Zhu, L.; Pei, A.; Wang, J.; Yang, K.; Zhang, C.; Xiao, S.; Chen, B.H. A highly selective and efficient Pd/Ni/Ni(OH)<sub>2</sub>/C catalyst for furfural hydrogenation at low temperatures. *Mol. Catal.* **2020**, *480*, 110639. [\[CrossRef\]](#)
14. Yuan, Q.; Zhang, D.; Haandel, L.V.; Ye, F.; Xue, T.; Hensen, E.J.M.; Guan, Y. Selective liquid phase hydrogenation of furfural to furfuryl alcohol by Ru/Zr-MOFs. *J. Mol. Catal. A Chem.* **2015**, *406*, 58–64. [\[CrossRef\]](#)
15. Nanao, H.; Murakami, Y.; Sato, O.; Yamaguchi, A.; Hiyoshi, N.; Shirai, M. Furfuryl alcohol and furfural hydrogenation over activated carbon-supported palladium catalyst in presence of water and carbon dioxide. *ChemistrySelect* **2017**, *2*, 2471–2475. [\[CrossRef\]](#)
16. Liu, L.; Lou, H.; Chen, M. Selective hydrogenation of furfural over Pt based and Pd based bimetallic catalysts supported on modified multiwalled carbon nanotubes (MWNT). *Appl. Catal. A Gen.* **2018**, *550*, 1–10. [\[CrossRef\]](#)
17. Li, S.; Wang, Y.; Gao, L.; Wu, Y.; Yang, X.; Sheng, P.; Xiao, G. Short channeled Ni-Co/SBA-15 catalysts for highly selective hydrogenation of biomass-derived furfural to tetrahydrofurfuryl alcohol. *Microporous Mesoporous Mater.* **2018**, *262*, 154–165. [\[CrossRef\]](#)
18. Nakagawa, Y.; Takada, K.; Tamura, M.; Tomishige, K. Total hydrogenation of furfural and 5-hydroxymethylfurfural over supported Pd–Ir alloy catalyst. *ACS Catal.* **2014**, *4*, 2718–2726. [\[CrossRef\]](#)
19. Nakagawa, Y.; Nakazawa, H.; Watanabe, H.; Tomishige, K. Total hydrogenation of furfural over a silica-supported nickel catalyst prepared by the reduction of a nickel nitrate precursor. *ChemCatChem* **2012**, *4*, 1791–1797. [\[CrossRef\]](#)
20. Huang, R.; Cui, Q.; Yuan, Q.; Wu, H.; Guan, Y.; Wu, P. Total hydrogenation of furfural over Pd/Al<sub>2</sub>O<sub>3</sub> and Ru/ZrO<sub>2</sub> mixture under mild conditions: Essential role of tetrahydrofurfural as an intermediate and support effect. *ACS Sustain. Chem. Eng.* **2018**, *6*, 6957–6964. [\[CrossRef\]](#)
21. Yin, D.; Ren, H.; Li, C.; Liu, J.; Liang, C. Highly selective hydrogenation of furfural to tetrahydrofurfuryl alcohol over MIL-101(Cr)-NH<sub>2</sub> supported Pd catalyst at low temperature. *Chin. J. Catal.* **2018**, *39*, 319–326. [\[CrossRef\]](#)
22. Sang, S.; Wang, Y.; Zhu, W.; Xiao, G. Selective hydrogenation of furfuryl alcohol to tetrahydrofurfuryl alcohol over Ni/γ-Al<sub>2</sub>O<sub>3</sub> catalysts. *Res. Chem. Intermed.* **2016**, *43*, 1179–1195. [\[CrossRef\]](#)
23. Liu, L.; Lou, H.; Chen, M. Selective hydrogenation of furfural to tetrahydrofurfuryl alcohol over Ni/CNTs and bimetallic CuNi/CNTs catalysts. *Int. J. Hydrogen Energy* **2016**, *41*, 14721–14731. [\[CrossRef\]](#)
24. Li, C.; Xu, G.; Liu, X.; Zhang, Y.; Fu, Y. Hydrogenation of biomass-derived furfural to tetrahydrofurfuryl alcohol over hydroxyapatite-supported Pd catalyst under mild conditions. *Ind. Eng. Chem. Res.* **2017**, *56*, 8843–8849. [\[CrossRef\]](#)
25. Wang, H.; Li, X.; Lan, X.; Wang, T. Supported ultrafine NiCo bimetallic alloy nanoparticles derived from bimetal-organic frameworks: A highly active catalyst for furfuryl alcohol hydrogenation. *ACS Catal.* **2018**, *8*, 2121–2128. [\[CrossRef\]](#)
26. Parikh, J.; Srivastava, S.; Jadeja, G.C. Selective hydrogenation of furfural to tetrahydrofurfuryl alcohol using supported nickel-cobalt catalysts. *Ind. Eng. Chem. Res.* **2019**, *58*, 16138–16152. [\[CrossRef\]](#)
27. Albilali, R.; Douthwaite, M.; He, Q.; Taylor, S.H. The selective hydrogenation of furfural over supported palladium nanoparticle catalysts prepared by sol-immobilisation: Effect of catalyst support and reaction conditions. *Catal. Sci. Technol.* **2018**, *8*, 252–267. [\[CrossRef\]](#)
28. Yang, Y.; Ma, J.; Jia, X.; Du, Z.; Duan, Y.; Xu, J. Aqueous phase hydrogenation of furfural to tetrahydrofurfuryl alcohol on alkaline earth metal modified Ni/Al<sub>2</sub>O<sub>3</sub>. *RSC Adv.* **2016**, *6*, 51221–51228. [\[CrossRef\]](#)
29. Cao, Y.; Zhang, H.; Liu, K.; Zhang, Q.; Chen, K.-J. Biowaste-derived bimetallic Ru–MoO<sub>x</sub> catalyst for the direct hydrogenation of furfural to tetrahydrofurfuryl alcohol. *ACS Sustain. Chem. Eng.* **2019**, *7*, 12858–12866. [\[CrossRef\]](#)
30. Pendem, S.; Bolla, S.R.; Morgan, D.J.; Shinde, D.B.; Lai, Z.; Nakka, L.; Mondal, J. Metal-organic-framework derived Co-Pd bond is preferred over Fe-Pd for reductive upgrading of furfural to tetrahydrofurfuryl alcohol. *Dalton Trans.* **2019**, *48*, 8791–8802. [\[CrossRef\]](#)
31. Ma, R.; Wu, X.-P.; Tong, T.; Shao, Z.-J.; Wang, Y.; Liu, X.; Xia, Q.; Gong, X.-Q. The critical role of water in the ring opening of furfural alcohol to 1,2-pentanediol. *ACS Catal.* **2016**, *7*, 333–337. [\[CrossRef\]](#)

32. Gao, F.; Liu, H.; Hu, X.; Chen, J.; Huang, Z.; Xia, C. Selective hydrogenolysis of furfuryl alcohol to 1,5- and 1,2-pentanediol over Cu-LaCoO<sub>3</sub> catalysts with balanced Cu<sup>0</sup>-CoO sites. *Chin. J. Catal.* **2018**, *39*, 1711–1723. [[CrossRef](#)]
33. Tong, T.; Liu, X.; Guo, Y.; Norouzi Banis, M.; Hu, Y.; Wang, Y. The critical role of CeO<sub>2</sub> crystal-plane in controlling Pt chemical states on the hydrogenolysis of furfuryl alcohol to 1,2-pentanediol. *J. Catal.* **2018**, *365*, 420–428. [[CrossRef](#)]
34. Date, N.S.; Chikate, R.C.; Roh, H.-S.; Rode, C.V. Bifunctional role of Pd/MMT-K 10 catalyst in direct transformation of furfural to 1,2-pentanediol. *Catal. Today* **2018**, *309*, 195–201. [[CrossRef](#)]
35. Zhang, B.; Zhu, Y.; Ding, G.; Zheng, H.; Li, Y. Selective conversion of furfuryl alcohol to 1,2-pentanediol over a Ru/MnOx catalyst in aqueous phase. *Green Chem.* **2012**, *14*, 3402. [[CrossRef](#)]
36. Sitthisa, S.; Pham, T.; Prasomsri, T.; Sooknoi, T.; Mallinson, R.G.; Resasco, D.E. Conversion of furfural and 2-methylpentanal on Pd/SiO<sub>2</sub> and Pd-Cu/SiO<sub>2</sub> catalysts. *J. Catal.* **2011**, *280*, 17–27. [[CrossRef](#)]
37. Wang, C.T.; Liu, Z.Q.; Wang, L.; Dong, X.; Zhang, J.; Wang, G.X.; Han, S.C.; Meng, X.J.; Zheng, A.M.; Xiao, F.S. Importance of zeolite wettability for selective hydrogenation of furfural over Pd@Zeolite catalysts. *ACS Catal.* **2018**, *8*, 474–481. [[CrossRef](#)]
38. Iqbal, S.; Liu, X.; Aldosari, O.F.; Miedziak, P.J.; Edwards, J.K.; Brett, G.L.; Akram, A.; King, G.M.; Davies, T.E.; Morgan, D.J.; et al. Conversion of furfuryl alcohol into 2-methylfuran at room temperature using Pd/TiO<sub>2</sub> catalyst. *Catal. Sci. Technol.* **2014**, *4*, 2280–2286. [[CrossRef](#)]
39. Zhang, L.; Meng, S.X.; Feng, Y.Q.; Zhang, B.; Xu, Z. A continuous process for the preparation of pyridine from tetrahydrofurfuryl alcohol with (MoO<sub>3</sub>-NiO)/Al<sub>2</sub>O<sub>3</sub> as Catalyst. *Adv. Mater. Res.* **2012**, *581–582*, 27–32.
40. Li, L.; Barnett, K.J.; McClelland, D.J.; Zhao, D.; Liu, G.; Huber, G.W. Gas-phase dehydration of tetrahydrofurfuryl alcohol to dihydropyran over  $\gamma$ -Al<sub>2</sub>O<sub>3</sub>. *Appl. Catal. B Environ.* **2019**, *245*, 62–70. [[CrossRef](#)]
41. Soghrati, E.; Choong, C.; Poh, C.K.; Kawi, S.; Borgna, A. Single-pot conversion of tetrahydrofurfuryl alcohol into tetrahydropyran over a Ni/HZSM-5 catalyst under aqueous-phase conditions. *ChemCatChem* **2017**, *9*, 1402–1408. [[CrossRef](#)]
42. Brentzel, Z.J.; Barnett, K.J.; Huang, K.; Maravelias, C.T.; Dumesic, J.A.; Huber, G.W. Chemicals from biomass: Combining ring-opening tautomerization and hydrogenation reactions to produce 1,5-pentanediol from furfural. *ChemSusChem* **2017**, *10*, 1351–1355. [[CrossRef](#)] [[PubMed](#)]
43. Wang, C.; Lee, J.D.; Ji, Y.; Onn, T.M.; Luo, J.; Murray, C.B.; Gorte, R.J. A study of tetrahydrofurfuryl alcohol to 1,5-pentanediol over Pt-WOx/C. *Catal. Lett.* **2018**, *148*, 1047–1054. [[CrossRef](#)]
44. Soghrati, E.; Kok Poh, C.; Du, Y.; Gao, F.; Kawi, S.; Borgna, A. C–O hydrogenolysis of tetrahydrofurfuryl alcohol to 1,5-pentanediol over bi-functional nickel-tungsten catalysts. *ChemCatChem* **2018**, *10*, 4652–4664. [[CrossRef](#)]
45. Liu, S.; Okuyama, Y.; Tamura, M.; Nakagawa, Y.; Imai, A.; Tomishige, K. Production of renewable hexanols from mechanocatalytically depolymerized cellulose by using Ir-ReOx/SiO<sub>2</sub> catalyst. *ChemSusChem* **2015**, *8*, 628–635. [[CrossRef](#)]
46. Huang, K.; Brentzel, Z.J.; Barnett, K.J.; Dumesic, J.A.; Huber, G.W.; Maravelias, C.T. Conversion of furfural to 1,5-pentanediol: Process synthesis and analysis. *ACS Sustain. Chem. Eng.* **2017**, *5*, 4699–4706. [[CrossRef](#)]
47. Yuan, Q.; Ye, F.; Xue, T.; Guan, Y. Room temperature hydrogenation of furfuryl alcohol by Pd/titanate nanotube. *Appl. Catal. A Gen.* **2015**, *507*, 26–33. [[CrossRef](#)]
48. Trzeciak, A.M.; Augustyniak, A.W. The role of palladium nanoparticles in catalytic C–C cross-coupling reactions. *Coord. Chem. Rev.* **2019**, *384*, 1–20. [[CrossRef](#)]
49. Sudarsanam, P.; Zhong, R.; Van den Bosch, S.; Coman, S.M.; Parvulescu, V.I.; Sels, B.F. Functionalised heterogeneous catalysts for sustainable biomass valorisation. *Chem. Soc. Rev.* **2018**, *47*, 8349–8402. [[CrossRef](#)]
50. Li, G.; Zhao, S.; Zhang, Y.; Tang, Z. Metal-organic frameworks encapsulating active nanoparticles as emerging composites for catalysis: Recent progress and perspectives. *Adv. Mater.* **2018**, *30*, 1800702. [[CrossRef](#)]
51. Yang, Q.; Xu, Q.; Jiang, H.L. Metal-organic frameworks meet metal nanoparticles: Synergistic effect for enhanced catalysis. *Chem. Soc. Rev.* **2017**, *46*, 4774–4808. [[CrossRef](#)] [[PubMed](#)]
52. Falcaro, P.; Ricco, R.; Yazdi, A.; Imaz, I.; Furukawa, S.; Maspoch, D.; Ameloot, R.; Evans, J.D.; Doonan, C.J. Application of metal and metal oxide nanoparticles@MOFs. *Coord. Chem. Rev.* **2016**, *307*, 237–254. [[CrossRef](#)]
53. Wang, Q.; Astruc, D. State of the art and prospects in metal–Organic framework (MOF)-based and MOF-derived nanocatalysis. *Chem. Rev.* **2019**. [[CrossRef](#)] [[PubMed](#)]

54. Duan, Y.; Zheng, M.; Li, D.; Deng, D.; Wu, C.; Yang, Y. Synthesis of Pd/SBA-15 catalyst employing surface-bonded vinyl as a reductant and its application in the hydrogenation of nitroarenes. *RSC Adv.* **2017**, *7*, 3443–3449. [[CrossRef](#)]
55. Duan, Y.; Zheng, M.; Li, D.; Deng, D.; Ma, L.-F.; Yang, Y. Conversion of HMF to methyl cyclopentenolone by the Pd/Nb<sub>2</sub>O<sub>5</sub> and Ca-Al catalysts via two-steps procedure. *Green Chem.* **2017**, *19*, 5103–5113. [[CrossRef](#)]
56. Yang, Y.; Xie, Y.; Deng, D.; Li, D.; Zheng, M.; Duan, Y. Highly selective conversion of HMF to 1-hydroxy-2,5-hexanedione on Pd/MIL-101(Cr). *ChemistrySelect* **2019**, *4*, 11165–11171. [[CrossRef](#)]
57. Yang, Y.; Xie, Y.; Zhang, J.; Li, D.; Deng, D.; Duan, Y. Fabrication of Pd/SiO<sub>2</sub> with controllable wettability for enhanced catalytic hydrogenation activity at ambient H<sub>2</sub> pressure. *ChemCatChem* **2019**, *11*, 5430–5434. [[CrossRef](#)]
58. Katz, M.J.; Brown, Z.J.; Colon, Y.J.; Siu, P.W.; Scheidt, K.A.; Snurr, R.Q.; Hupp, J.T.; Farha, O.K. A facile synthesis of UiO-66, UiO-67 and their derivatives. *Chem. Commun.* **2013**, *49*, 9449–9451. [[CrossRef](#)]
59. Shen, L.; Wu, W.; Liang, R.; Lin, R.; Wu, L. Highly dispersed palladium nanoparticles anchored on UiO-66(NH<sub>2</sub>) metal-organic framework as a reusable and dual functional visible-light-driven photocatalyst. *Nanoscale* **2013**, *5*, 9374. [[CrossRef](#)]
60. Guan, Q.; Wang, B.; Chai, X.; Liu, J.; Gu, J.; Ning, P. Comparison of Pd-UiO-66 and Pd-UiO-66-NH<sub>2</sub> catalysts performance for phenol hydrogenation in aqueous medium. *Fuel* **2017**, *205*, 130–141. [[CrossRef](#)]
61. Brun, M.; Berthet, A.; Bertolini, J.C. XPS, AES and Auger parameter of Pd and PdO. *J. Electron Spectrosc. Relat. Phenom.* **1999**, *104*, 55–60. [[CrossRef](#)]



© 2019 by the authors. Licensee MDPI, Basel, Switzerland. This article is an open access article distributed under the terms and conditions of the Creative Commons Attribution (CC BY) license (<http://creativecommons.org/licenses/by/4.0/>).